Perturbation analysis of mixing and dispersion regimes in the low and intermediate Péclet number region

M. Giona* and S. Cerbelli
Dipartimento di Ingegneria Chimica, Sapienza Università di Roma, via Eudossiana 18, 00184 Roma, Italy
(Received 19 October 2009; revised manuscript received 20 January 2010; published 13 April 2010)

The object of this paper is to show that a variety of dispersion and mixing phenomena induced by laminar convection and diffusion can be approached by perturbation analysis of the spectrum associated with the corresponding advection-diffusion operator. As a case study for dispersion, we consider the classical Taylor-Aris problem, whereas a prototypical model of Sturm-Liouville generalized eigenvalue problem is considered for describing mixing in open or closed bounded flows. For both cases, we show how a simplified (low-order) perturbative approach defines quantitatively the range of different mixing regimes and the associated time scales. Furthermore, we show how a complete higher-order approach cannot improve significantly the simplified low-order analysis due to the lack of analyticity of the eigenvalue branches. The perturbation analysis is also extended to models of physically realizable mixing systems (lid-driven cavity flow).

DOI: 10.1103/PhysRevE.81.046309 PACS number(s): 47.15.−x, 83.50.Ha, 83.50.Rp, 05.60.−k

I. INTRODUCTION

Triggered by the technological development of microsystem engineering [1] and by the broad range of different physical phenomenologies it can embrace [2], the analysis of the dynamics of scalar fields advected by a regular flow in the presence of molecular diffusion is experiencing continuous advances.

In recent years, it became clear that complex transport phenomenologies can arise not only in kinematically complex flows (such as those giving rise to Lagrangian chaos), but even in simple flows that are trivial from the kinematic standpoint [3]. This is, for example, the case of the scaling of the mixing layer in T-junction microdevices [4] of the dispersion properties in straight capillaries and finite length microchannels at high values of the Péclet number [5] (the Péclet number $\mathrm{Pe}=t_{\mathrm{dif}}/t_{\mathrm{adv}}$ is the ratio of the characteristic time for diffusion t_{dif} to that of advection t_{adv}; in the case of parallel channel flows of finite length L, $t_{\mathrm{dif}}=L^2/D$, where D is the solute diffusivity, $t_{\mathrm{adv}}=L/V$, where V is the mean axial velocity, so that $\mathrm{Pe}=VL/D$), beyond the region of validity of Taylor-Aris dispersion theory [6].

Similarly, in the investigation of mixing properties of simple flow systems in the presence of molecular diffusion, recent studies have unveiled a complex spectral structure of the non-Hermitian advection-diffusion operator that controls the decays of scalar norms [7]. This analysis is particularly interesting for high values of the Péclet number, where the occurrence of different mixing regimes is associated with different asymptotic scalings of the real part of the eigenvalue spectrum as a function of the Péclet number.

In this paper, we analyze the capability of perturbation methods to predict mixing and dispersion properties in the low and intermediate ranges of the Péclet number, starting from the analysis of the eigenvalue spectrum of the advection-diffusion operator. Specifically, the main focus of this are is (i) to show that simplified perturbative approaches, based on the physical definition of different mixing regimes, can predict with sufficient accuracy the leading-order behavior of the eigenvalue spectrum for low and intermediate Péclet numbers, (ii) to relate these simplified approaches to the properties of the eigenfunctions in the low Péclet number region, and (iii) to develop a complete perturbative analysis, similar to the classical perturbation technique developed in quantum mechanics, of the non-Hermitian operators associated with the interplay between advection and diffusion both in steady and unsteady, and batch and open mixing systems.

The paper is organized as follows. Section II presents an alternative spectral derivation of the Taylor-Aris dispersion theory in the presence of cross-sectional flows. In point of fact, dispersion theory in long channel can be viewed as a perturbative problem and different perturbative schemes have been proposed [8]. We propose a simple approach that unifies the analysis of dispersion with the spectral analysis of mixing in closed and open systems. Section III discusses mixing regimes in simple flow systems. From the physical understanding of the dominant contribution to mixing, a simplified perturbative approach is developed. Section IV addresses a nonapproximate perturbative approach, compares its results to the method developed in Sec. III, and discusses its range of validity. Moreover, the perturbation analysis is extended to a typical, physically realizable flow system, namely, the lid-driven cavity flow.

II. SPECTRAL VIEW TO TAYLOR-ARIS DISPERSION

This section reformulates the Taylor-Aris theory for infinitely long straight channels as a simple perturbation problem for the eigenvalue spectrum of the advection-diffusion operator in laminar incompressible flows. Let $\mathbf{x}_\perp$ be the dimensionless transverse coordinate vector, normalized with respect to the characteristic transverse length W and $\tau=tD/W^2$ the dimensionless time (D is solute molecular diffusivity). Let $\Sigma_\perp$ be the channel cross section in the dimensionless coordinate system.

*Author to whom correspondence should be addressed; max@giona.ing.uniroma1.it

Let us suppose that the velocity field consists of an axial component $v_z(\mathbf{x}_\perp)=V[1+\chi(\mathbf{x}_\perp)]$ (V is the mean axial velocity) and of a cross-sectional component $V_\perp \mathbf{u}(\mathbf{x}_\perp)$, which depends solely on the cross-sectional coordinates $\mathbf{x}_\perp$. By definition of $\chi(\mathbf{x}_\perp)$, it follows that $\int_{\Sigma_\perp}\chi(\mathbf{x}_\perp)dS=0$. In the classical Taylor-Aris theory, the cross-sectional velocity contribution is absent ($V_\perp=0$). Besides, this additional term can describe simple transverse electro-osmotic flows in microdevices [9], which are superimposed to the pressure-driven axial flow.

In a reference frame moving with the average axial velocity V, the balance equation for the dimensionless solute concentration ϕ within the capillary reads

$$\frac{\partial \phi}{\partial \tau} = -\mathrm{Pe}\chi\frac{\partial \phi}{\partial \zeta} - \mathrm{Pe}_\perp \mathbf{u}\cdot\nabla_\perp \phi + \nabla_\perp^2 \phi + \frac{\partial^2 \phi}{\partial \zeta^2}, \tag{1}$$

where ζ is the axial coordinate in the moving reference system, $\tau=tD/W^2$ (t is the physical time), $\mathrm{Pe}=VW/D$, $\mathrm{Pe}_\perp=V_\perp W/D$, and $\nabla_\perp$ is the cross-sectional nabla operator (with respect to the transverse coordinates $\mathbf{x}_\perp$). Equation (1) is equipped with the Neumann boundary condition $\partial\phi/\partial n|_{\partial\Sigma_\perp}=0$ at the boundary $\partial\Sigma_\perp$ of the cross section. For $\mathrm{Pe}_\perp=0$, Eq. (1) provides the classical formulation of the dispersion problem in long channels due to Aris [6], which is customarily approached by means of moment analysis.

To state that the interplay between the flow field and molecular diffusion gives rise to the occurrence of an effective dispersion coefficient D_{dis}, which is the essence of the argument of Taylor and Aris, is equivalent to say that in the long-time, long-distance asymptotics, the evolution of the sectionally averaged solute concentration $\bar{\phi}(\tau,\zeta)=1/\mathrm{area}(\Sigma_\perp)\int_{\Sigma_\perp}\phi dS$ can be described as a purely diffusive transport problem

$$\frac{\partial \bar{\phi}}{\partial \tau} = \hat{D}_{\mathrm{dis}}\frac{\partial^2 \bar{\phi}}{\partial \zeta^2}, \tag{2}$$

where $\hat{D}_{\mathrm{dis}}=D_{\mathrm{dis}}/D$ is the dimensionless dispersion coefficient. The interplay between advection and diffusion in long tubes, which controls the broadening of concentration profiles, is therefore completely embedded in the functional form of the effective dispersion coefficient $\hat{D}_{\mathrm{dis}}$ and in its dependence on the Péclet number.

Since, by hypothesis, the channel is infinitely extended, $\zeta\in(-\infty,\infty)$, the scalar field $\phi(\tau,\mathbf{x}_\perp,\zeta)$ can be expressed via a Fourier transform

$$\phi(\tau,\mathbf{x}_\perp,\zeta) = \int_{-\infty}^{\infty} e^{ik\zeta}\phi_k(\tau,\mathbf{x}_\perp)dk, \tag{3}$$

where $i=\sqrt{-1}$. The dynamics of each mode ϕ_k satisfies the equation

$$\frac{\partial \phi_k}{\partial \tau} = -ik\ \mathrm{Pe}\ \chi\phi_k - \mathrm{Pe}_\perp \mathbf{u}\cdot\nabla_\perp \phi_k + \nabla_\perp^2 \phi_k - k^2\phi_k = \mathcal{L}_k[\phi_k]. \tag{4}$$

If Eq. (2) holds in the long-distance limit, then the eigenvalues λ_k of the linear operator $\mathcal{L}_k$ at the right-hand side of Eq. (4),

$$\lambda_k\psi_k = -ik\ \mathrm{Pe}\ \chi\psi_k - \mathrm{Pe}_\perp \mathbf{u}\cdot\nabla_\perp \psi_k + \nabla_\perp^2 \psi_k - k^2\psi_k, \tag{5}$$

must verify the condition

$$\lambda_k = -k^2\hat{D}_{\mathrm{dis}} + \mathcal{O}(k^3), \quad k\in(-\infty,\infty) \tag{6}$$

in the limit of small k (long-distance approximation). Let $\mu_k=\lambda_k+k^2$, so that Eq. (6) becomes

$$\mu_k\psi_k(\mathbf{x}_\perp) = -ik\ \mathrm{Pe}\ \chi(\mathbf{x}_\perp)\psi_k(\mathbf{x}_\perp) - \mathrm{Pe}_\perp \mathbf{u}(\mathbf{x}_\perp)\cdot\nabla_\perp \psi_k(\mathbf{x}_\perp) + \nabla_\perp^2 \psi_k(\mathbf{x}_\perp). \tag{7}$$

Expanding μ_k and ψ_k in power series of Pe,

$$\mu_k = \mu_{k,0} + \mathrm{Pe}\ \mu_{k,1} + \mathrm{Pe}^2\mu_{k,2} + \cdots, \tag{8}$$

$$\psi_k = \psi_{k,0} + \mathrm{Pe}\ \psi_{k,1} + \mathrm{Pe}^2\psi_{k,2} + \cdots, \tag{9}$$

and substituting this expansion into Eq. (7), one obtains

$$\mu_{k,0}\psi_{k,0} = -\mathrm{Pe}_\perp \mathbf{u}\cdot\nabla_\perp \psi_{k,0} + \nabla_\perp^2 \psi_{k,0}, \tag{10}$$

$$\mu_{k,1}\psi_{k,0} + \mu_{k,0}\psi_{k,1} = -ik\chi\psi_{k,0} - \mathrm{Pe}_\perp \mathbf{u}\cdot\nabla_\perp \psi_{k,1} + \nabla_\perp^2 \psi_{k,1}, \tag{11}$$

$$\mu_{k,2}\psi_{k,0} + \mu_{k,1}\psi_{k,1} + \mu_{k,0}\psi_{k,2} = -ik\chi\psi_{k,1} - \mathrm{Pe}_\perp \mathbf{u}\cdot\nabla_\perp \psi_{k,2} + \nabla_\perp^2 \psi_{k,2}, \tag{12}$$

equipped with the Neumann boundary conditions $\partial\psi_{k,h}/\partial n|_{\partial\Sigma_\perp}=0$, $h=0,1,\ldots$.

The dominant eigenvalue of the zeroth order perturbation is $\mu_{k,0}=0$ and the corresponding eigenfunction is $\psi_{k,0}=1$. By definition, the dominant eigenvalue (of the whole spectrum or of a specific spectral branch) is the eigenvalue with the largest absolute value of the real part, which dominates the asymptotic exponential decay for generic initial conditions (in the case of the whole spectrum) or for generic initial conditions exciting solely a given spectral branch (in the case of a spectral branch).

Substituting this result into the equation for the first-order term, one obtains

$$\nabla_\perp^2 \psi_{k,1} - \mathrm{Pe}_\perp \mathbf{u}(\mathbf{x}_\perp)\cdot\nabla_\perp \psi_{k,1} = \mu_{k,1} + ik\chi(\mathbf{x}_\perp). \tag{13}$$

Note that, because of the homogeneous Neumann boundary conditions, a necessary requirement for the existence of a solution of Eq. (13) is that the forcing term $\mu_{k,1}+ik\chi(\mathbf{x}_\perp)$ possesses vanishing cross-sectional mean value. This implies that

$$\int_{\Sigma_\perp}[\mu_{k,1} + ik\chi(\mathbf{x}_\perp)]dS = 0 \Rightarrow \mu_{k,1} = 0 \tag{14}$$

and therefore the corresponding eigenfunction term satisfies the elliptic equation

$$\nabla_\perp^2 \psi_{k,1} - \mathrm{Pe}_\perp \mathbf{u}(\mathbf{x}_\perp)\cdot\nabla_\perp \psi_{k,1} = ik\chi(\mathbf{x}_\perp). \tag{15}$$

For the second-order term, one obtains

$$\nabla_\perp^2 \psi_{k,2} - \mathrm{Pe}_\perp \mathbf{u}(\mathbf{x}_\perp)\cdot\nabla_\perp \psi_{k,2} = \mu_{k,2} + ik\chi(\mathbf{x}_\perp)\psi_{k,1} \quad (16)$$

Also, for Eq. (16), a solution exists if and only if $\mu_{k,2} + ik\chi(\mathbf{x}_\perp)\psi_{k,1}$ admits vanishing cross-sectional average, i.e.,

$$\mu_{k,2} = -\frac{ik}{\mathrm{area}(\Sigma_\perp)}\int_{\Sigma_\perp} \chi(\mathbf{x}_\perp)\psi_{k,1}(\mathbf{x}_\perp)dS, \quad (17)$$

which provides the second-order correction. Letting $\psi_{k,1} = -ikg_1$, the function $g_1(\mathbf{x}_\perp)$ satisfies the elliptic equation

$$\nabla_\perp^2 g_1 - \mathrm{Pe}_\perp \mathbf{u}(\mathbf{x}_\perp)\cdot\nabla_\perp g_1 = -\chi(\mathbf{x}_\perp) \quad (18)$$

and

$$\mu_{2,k} = -k^2\overline{\chi g_1}, \quad \overline{\chi g_1} = \frac{1}{\mathrm{area}(\Sigma_\perp)}\int_{\Sigma_\perp} \chi(\mathbf{x}_\perp)g_1(\mathbf{x}_\perp)dS. \quad (19)$$

Equations (8) and (19) imply that

$$\mu_k = -k^2\,\mathrm{Pe}^2\overline{\chi g_1}, \quad (20)$$

which implies that Eq. (6) is satisfied, since

$$\lambda_k = -k^2 - k^2\,\mathrm{Pe}^2\overline{\chi g_1} = -k^2(1+\mathrm{Pe}^2\Gamma_{\mathrm{TA}}) \quad (21)$$

where $\Gamma_{\mathrm{TA}} = \overline{\chi g_1}$ is the generalized Taylor-Aris dispersion coefficient. It is straightforward to check from Eq. (18) that $\Gamma_{\mathrm{TA}} \geq 0$. Equation (21) enables us to identify the effective dispersion coefficient D_{dis},

$$D_{\mathrm{dis}} = D + \frac{V^2W^2\Gamma_{\mathrm{TA}}}{D}. \quad (22)$$

For $\mathrm{Pe}_\perp = 0$, one recovers the classical Taylor-Aris expression, usually derived by means of moment analysis [6]. For $\mathrm{Pe}_\perp \neq 0$, one obtains a simple and rigorous derivation of the expression obtained in [10] in the presence of cross-sectional velocity fields.

III. MIXING REGIMES: ANGULAR DIFFUSION AND SIMPLIFIED PERTURBATIONS

This section analyzes the behavior of the mixing regimes in the low and intermediate Péclet number regions and the development of simplified perturbation techniques that can be deduced from the physical insight on the properties of these regimes.

A. Model problem

Henceforth, we consider the following generalized eigenvalue-eigenfunction problem

$$\lambda w(y)\psi(y) = \varepsilon\partial_y^2\psi(y) + iV(y)\psi(y) - \varepsilon\frac{4\pi^2}{\alpha_m^2}\psi(y), \quad (23)$$

where $y \in (0,1)$ and $\psi(y)$ is equipped with the homogeneous Neumann conditions $\partial_y\psi(y)|_{y=0,1} = 0$. In Eq. (23), $w(y) \geq 0$, α_m is a real parameter, and $\varepsilon = 1/\mathrm{Pe}_{\mathrm{eff}}$ is the reciprocal of the "effective Péclet number" (see below for details).

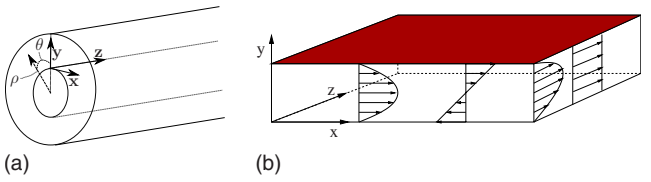

FIG. 1. (Color online) (a) Couette system in a cylindrical coordinate system (ρ,θ,z). (b) Schematic representation of the geometry of the rectified Couette flow. In the rectified model $\rho \mapsto y$, $\theta \mapsto x$, and $z \mapsto z$. Since x corresponds to a rectified angular coordinate, periodic boundary conditions are imposed at $x = 0, L_x$. Several velocity profiles considered throughout the paper are schematically depicted.

The physical basis of Eq. (23) is the stationary response of a rectified version of the inflow-outflow Couette system [see Fig. 1(a)], depicted in Fig. 1(b), where $x \in (0,L_x)$, $y \in (0,L_y)$, $z \in (0,L_z)$, corresponding to the flow between two parallel plates located at $y=0$ and $y=1$. In this model, the coordinates x and z parametrize the angular and axial directions, respectively (periodic boundary conditions are imposed between $x=0$ and $x=L_x$), the axial profile $v_z(y)$ is a pressure-driven Poiseuille flow (unless otherwise stated), and the "angular" profile $v_x(y)$ represents the planar Couette flow induced by the motion of the lower and upper walls, $y=0$ and $y=1$.

In stationary conditions, the equation for the propagation of a scalar field ϕ along the channel is

$$v_z(y)\partial_z\phi = -v_x(y)\partial_x\phi + D(\partial_x^2\phi + \partial_y^2\phi + \partial_z^2\phi), \quad (24)$$

where D is the diffusion coefficient. Let $v_z(y) = V_\parallel w(y)$ and $v_x(y) = V_\perp u(y)$, where $V_\parallel$ and $V_\perp$ are the characteristic axial and cross-sectional velocities, respectively [$V_\parallel$ can be defined so that the dimensionless mean axial velocity $v_z(y)/V_\parallel$ equals 1], and let $x \to x/L_x$, $y \to y/L_y$, and $z \to z/L_z$. Henceforth, we let x, y, and z indicate the rescaled dimensionless variables. In this dimensionless setting, Eq. (23) becomes

$$w(y)\partial_z\phi = -\Gamma u(y)\partial_x\phi + \frac{\beta^2}{\mathrm{Pe}\,\alpha^2}\partial_x^2\phi + \frac{\beta^2}{\mathrm{Pe}}\partial_y^2\phi + \frac{1}{\mathrm{Pe}}\partial_z^2\phi, \quad (25)$$

where $\Gamma = V_\perp L_z/V_\parallel L_x$ measures the relative intensity of angular to axial velocity, $\mathrm{Pe} = V_\parallel L_z/D$ is the Péclet number, and α, β are the geometric aspect ratios $\alpha = L_x/L_y$, $\beta = L_z/L_x$. Since the aspect ratio β is usually much larger than 1, the effect of the axial diffusion can be neglected compared to transverse diffusion, so that Eq. (25) simplifies to

$$w(y)\partial_z\phi = -\Gamma u(y)\partial_x\phi + \varepsilon\partial_y^2\phi + \frac{\varepsilon}{\alpha^2}\partial_x^2\phi, \quad (26)$$

where

$$\varepsilon = \frac{1}{\mathrm{Pe}_{\mathrm{eff}}}, \quad \mathrm{Pe}_{\mathrm{eff}} = \frac{\mathrm{Pe}}{\beta^2}. \quad (27)$$

Expanding ϕ with respect to the periodic basis $e^{i2\pi mx}$, i.e., $\phi(x,y,z) = \Sigma_m \phi_m(y,z)e^{i2\pi mx}$, one obtains for ϕ_m the equation

TABLE I. Physical meaning of the terms appearing in Eq. (23) in the case of the steady response of an open (inflow-outflow) Couette mixing system.

Term	Physical meaning
$-w(y)\psi(y)$	Axial flow
$\varepsilon\partial_y^2\psi(y)$	Transverse diffusion
$iV(y)\psi(y)$	Transverse flow
$-\varepsilon(4\pi^2/\alpha_m^2)\psi(y)$	Angular diffusion

$$w(y)\partial_z\phi_m = iV(y)\phi_m + \varepsilon\partial_y^2\phi_m - \varepsilon\frac{4\pi^2}{\alpha_m^2}\phi_m, \qquad (28)$$

where $V(y)=-2\pi m\Gamma u(y)$ and $\alpha_m=\alpha/m$. Equation (28) gives rise to the eigenvalue problem expressed by Eq. (23). Table I reviews the physical meaning of each term entering Eq. (23) with reference to the three-dimensional inflow-outflow Couette system.

The eigenvalue problem Eq. (23) has been derived for a Cartesian version of the three-dimensional inflow-outflow Couette system under stationary conditions. It describes the stationary propagation of a scalar field in a cylindrical structure in the case where the gap between the inner (R_{in}) and the outer (R_{out}) radii is small, i.e., $1-R_{\text{in}}/R_{\text{out}}\ll 1$. In this problem, the eigenvalues λ are associated with the axial decay of the field norms (L^2, Sobolev norms) along the axial coordinate z. Physically meaningful expressions for $w(y)$ and $V(y)$ are $w(y)=6y(1-y)$ (corresponding to a Poiseuille axial flow) and $w(y)=2y$ (corresponding to a shear flow in the axial direction). For $V(y)$, we assume the expression $V(y)=-1+2y$, corresponding to equal counter-rotating motion of the walls. The value of the aspect ratio α (and, consequently of α_m, if one is interested in the dominant mode $m=1$) is much greater than 1.

In point of fact, the case $w(y)=1$ is also interesting, as Eq. (23) corresponds to the eigenvalue problem associated with the time evolution of a scalar field in a two-dimensional annular structure between two cylinders (in the small gap limit). In the latter case, the real parts of the eigenvalues λ correspond to the characteristic temporal decay rates of the norms of ϕ.

B. Mixing regimes

This section analyzes the occurrence and the physics of different mixing regimes in the low and intermediate Péclet number regions. Consider Eq. (23) for a Poiseuille flow $w(y)=6y(1-y)$ and for $V(y)=-1+2y$, corresponding to a transverse counter-rotating Couette flow. Let $\lambda=\mu+i\omega$ and μ_d the real part of the dominant eigenvalue, i.e., of the eigenvalue with the largest real part (since $\mu_d<0$, μ_d possesses the smallest absolute value).

Figure 2 depicts the behavior of the real part of the dominant eigenvalue with reverse sign as a function of the effective Péclet number $\text{Pe}_{\text{eff}}=\varepsilon^{-1}$ for several values of α_m [11]. As can be observed, for $\text{Pe}_{\text{eff}}\ll 1$, $-\mu_d$ is proportional to the reciprocal of the effective Péclet number [lines (a)–(c) in Fig. 2]. Although log-log scale is used in Fig. 2, observe that lines

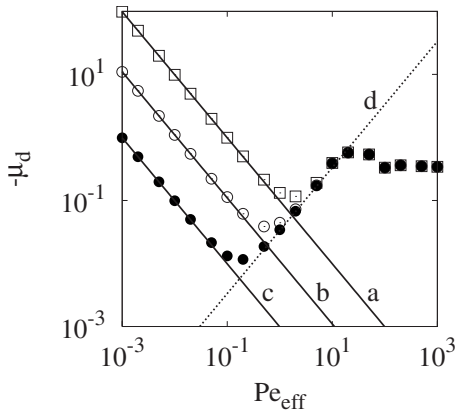

FIG. 2. Real part of the dominant eigenvalue with reversed sign $-\mu_d$ vs Pe_{eff} for a Poiseuille flow $w(y)=6y(1-y)$ and $V(y)=-1+2y$. Symbols (□), (○), and (●) refer to $\alpha_m=20$, $\alpha_m=60$, and $\alpha_m=200$, respectively. Lines (a)–(c) represent the angular diffusion scaling $-\mu_d=4\pi^2/(\alpha_m^2\,\text{Pe}_{\text{eff}})$. Dotted line (d) is the perturbative result deriving from Eq. (54) $-\mu_d=G^{(1)}(1)\,\text{Pe}_{\text{eff}}$, with $G^{(1)}(1)=0.0333$.

(a)–(c) correspond to $-\mu_d\sim 1/\text{Pe}_{\text{eff}}$. This phenomenon can be interpreted by observing that in this Péclet number region the homogenization of the scalar field is almost exclusively controlled by angular diffusion, i.e., by the diagonal term $-\varepsilon(4\pi^2/\alpha_m^2)\psi(y)$ entering Eq. (23). This stems from the fact that in the low Péclet region, the eigenfunctions are almost uniform and therefore $|\partial_y^2\psi(y)|\ll(4\pi^2/\alpha_m^2)|\psi(y)|$.

The action of pure angular diffusion in the absence of cross-sectional flow and in the presence of a uniform axial flow gives rise to a dominant eigenvalue equal to

$$-\lambda_d=-\mu_d=\frac{4\pi^2}{\alpha_m^2\text{Pe}_{\text{eff}}}. \qquad (29)$$

Lines (a)–(c) in Fig. 2 represent the diffusive scaling Eq. (29) and are fairly accurate descriptions of the spectral properties in the low Péclet number region to the leading order (see below for a quantification of this statement). This means that the spatial nonuniformities in the axial velocity profiles do not contribute, to the leading order, to the scaling of the dominant eigenvalue. This means that the characteristic decay $-\mu_d$ in this Péclet number region can be approximated by Eq. (29) as if $w(y)$ were spatially uniform (this issue is further addressed below).

As Pe_{eff} increases, a nonmonotonic behavior of $-\mu_d$ occurs: above the local minimum, the real part of the dominant eigenvalue (with reversed sign) grows proportionally to Pe_{eff}. Observe that above the local minimum, the values of $-\mu_d$ becomes practically independent of α_m. Physically, this means that the effect of angular diffusion is practically negligible in this parameter region. This phenomenon can be investigated further by considering a shear flow, i.e., $w(y)=2y$, for which analytical results can be obtained (see below).

Figure 3 (symbols ●) depicts the dominant eigenvalue $-\mu_d$ for the shear flow [and for $V(y)=-1+2y$]. The qualitative properties of $-\mu_d$ are similar to those characterizing the

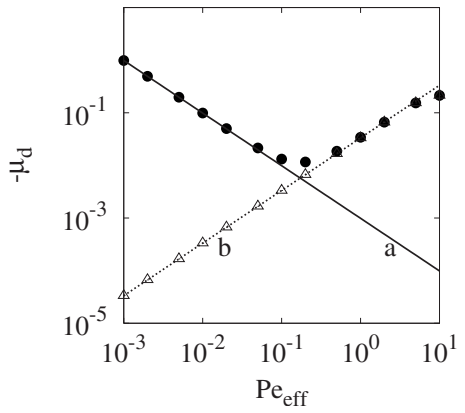

FIG. 3. Real part of the dominant eigenvalue with reversed sign $-\mu_d$ vs $\mathrm{Pe}_{\mathrm{eff}}$ for a shear flow $[w(y)=2y,\ V(y)=-1+2y]$. Symbols (●) refer to $\alpha_m=200$, while symbols (△) refer to the same problem in the absence of angular diffusion, Eq. (23) for $\alpha_m\to\infty$. Line (a) represents the angular diffusion scaling $-\mu_d=4\pi^2/(\alpha_m^2\,\mathrm{Pe}_{\mathrm{eff}})$, dotted line (b) is the perturbative result deriving from Eq. (54) $-\mu_d=G^{(1)}(1)\,\mathrm{Pe}_{\mathrm{eff}}$, with $G^{(1)}(1)=0.0333$.

Poiseuille flow depicted in Fig. 2. Figure 3 also depicts the dominant eigenvalue for $\alpha_m\to\infty$, corresponding to the eigenvalue problem Eq. (23) in the absence of angular diffusion (symbols △). In the limit for $\alpha_m\to\infty$, the whole low and intermediate Péclet numbers region is characterized by a dominant eigenvalue that is proportional to $\mathrm{Pe}_{\mathrm{eff}}$ and, more significantly, the eigenvalues for $\alpha_m\to\infty$ match quantitatively the corresponding eigenvalues for finite α_m for $\mathrm{Pe}_{\mathrm{eff}}$ values above the local minimum point, i.e., for $\mathrm{Pe}_{\mathrm{eff}}>10^{-1}$. The latter observation is particularly significant, since it enables us to apply a simple and effective perturbation expansion (see next subsection) grounded on the decoupling of the action of angular diffusion from the controlling homogenization dynamics.

Before developing such a simplified perturbation approach, it is interesting to analyze further the properties of the eigenvalues and eigenfunctions of Eq. (23). For $\mathrm{Pe}_{\mathrm{eff}}<10^{-1}$, the effect of the transverse velocity field $V(y)$ is practically negligible, so that the eigenvalue problem Eq. (23) simplifies to

$$\lambda w(y)\chi(y)=\varepsilon\partial_y^2\chi(y)-\varepsilon\frac{4\pi^2}{\alpha_m^2}\chi(y), \tag{30}$$

equipped with the homogeneous Neumann boundary conditions $\chi(y)|_{y=0,1}$. We use a different symbol, $\chi(y)$, instead of $\psi(y)$, to indicate the eigenfunctions of the simplified eigenvalue problem in which the effect of the transverse flow is neglected. The eigenvalues λ of Eq. (30) are all real (since the associated operator is Hermitian) and negative and the effect of the Péclet number can be scaled out by defining $\nu=\lambda/\varepsilon$.

Consider the case of a shear flow $w(y)=2y$, so that Eq. (30) becomes

$$(2\nu y+c)\chi(y)=\partial_y^2\chi(y), \tag{31}$$

where $c=4\pi^2/\alpha_m^2$. Let $\nu_a=-\nu>0$,

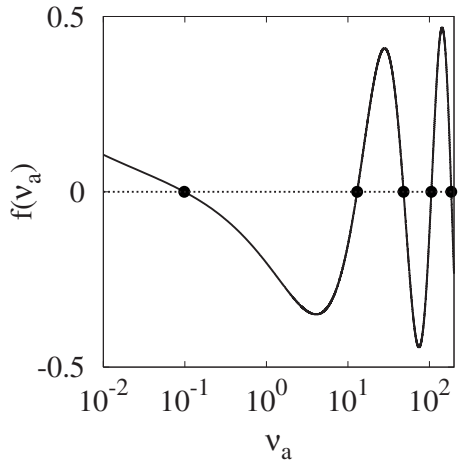

FIG. 4. Characteristic function $f(\nu_a)$ vs ν_a for the shear flow $[w(y)=2y]$ at $\alpha_m=20$. Dots (●) are the first zeroes of $f(\nu_a)$.

$$p=\frac{c}{2\nu_a},\quad q=-\left(\frac{1}{2\nu_a}\right)^{1/3},\quad \xi=\frac{y-p}{q}=\xi(y,\nu_a), \tag{32}$$

the eigenvalues ν_a (with reversed sign) satisfy the characteristic equation

$$f(\nu_a)=\mathrm{Ai}'[\xi_1(\nu_a)]\mathrm{Bi}'[\xi_2(\nu_a)]-\mathrm{Ai}'[\xi_2(\nu_a)]\mathrm{Bi}'[\xi_1(\nu_a)]=0, \tag{33}$$

where $\mathrm{Ai}(\xi)$ and $\mathrm{Bi}(\xi)$ are the Airy functions of the first and second kinds, $\mathrm{Ai}'(\xi_1)=d\,\mathrm{Ai}(\xi)/d\xi|_{\xi=\xi_1}$, and

$$\xi_1=\frac{c}{(2\nu_a)^{2/3}},\quad \xi_2=-\left[(2\nu_a)^{1/3}-\frac{c}{(2\nu_a)^{2/3}}\right]. \tag{34}$$

Equation (34) admits a countable system of positive roots $\nu_{a,h}$ $h=1,2,\ldots$, ordered in an increasing way with respect to h (see Fig. 4), that correspond to the eigenvalues ν_h with reversed sign. The associated eigenfunctions read as

$$\chi_h(y)=C_h\left[\mathrm{Ai}(\xi)-\frac{\mathrm{Ai}'(\xi_1)}{\mathrm{Bi}'(\xi_1)}\mathrm{Bi}(\xi)\right],\quad \xi=\xi(y,\nu_{c,h}),$$

$$h=1,2,\ldots, \tag{35}$$

where ξ depends on y and $\nu_{a,h}$ according to Eq. (32). Let us compare the eigenvalues $\nu=\lambda/\varepsilon$ of Eq. (30) to those obtained by considering exclusively the effect of the angular diffusion, the dominant eigenvalue of which (with reversed sign) is given by

$$g_d(\alpha_m)=\frac{4\pi^2}{\alpha_m^2}=c. \tag{36}$$

Figure 5 shows the behavior of $\nu_{a,1}(\alpha)$ and of the difference $g_d(\alpha_m)-\nu_{a,1}(\alpha_m)$ as a function of the aspect ratio α_m for the shear flow (panel A). It can be observed that $g_d(\alpha_m)$ represents the leading-order term in the expansion of $\nu_{a,1}(\alpha_m)$ as a function of $1/\alpha_m$. The second-order correction behaves quartically with α_m^{-1} [curve (b) and symbols (□)], i.e.,

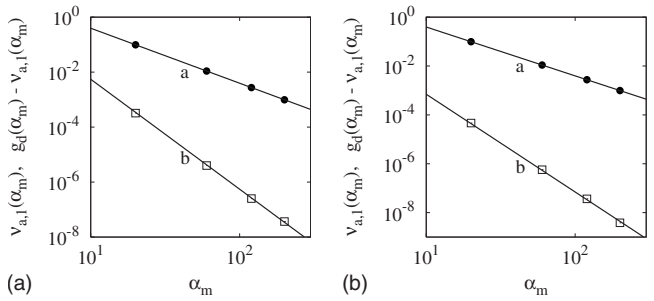

FIG. 5. $\nu_{a,1}(\alpha_m)$ [symbols (●)] and $g_d(\alpha_m)-\nu_{a,1}(\alpha_m)$ [symbols (□)] vs α_m for the shear flow (panel A) and for the Poiseuille flow (panel B). Lines (a) represent the function $g_d(\alpha_m)=4\pi^2/\alpha_m^2$, lines (b) the second-order correction to the eigenvalue scaling, $g_d(\alpha_m)-\nu_{a,1}(\alpha_m)=C_d/\alpha_m^4$.

$$\nu_{a,1}(\alpha_m) = g_d(\alpha_m) - \frac{C_d}{\alpha_m^4} + \mathcal{O}(\alpha_m^{-6}), \tag{37}$$

where $C_d>0$. An analogous result is obtained for the Poiseuille flow $w(y)=6y(1-y)$ [panel (b) of Fig. 5], although in the latter case no analytic expression for the eigenvalues $\nu_{a,1}(\alpha_m)$ is available. Note that this result implies that the effects of a nonuniform axial flow $w(y)$ (be it a shear or a Poiseuille profile) must be balanced, to the leading order, by the term $\partial_y^2\chi_1(y)$, so that the overall effect yields Eq. (37).

Figure 6 shows the profile of the dominant eigenfunction $\chi_1(y)$ for several values of α_m for the shear flow. As can be observed, the eigenfunctions are almost uniform (see the y range in Fig. 6). This result is a direct consequence of the relation between the eigenvalue and the norms of the associated eigenfunction. From Eq. (30), by considering the dominant eigenfunction normalized with respect to the weighted L^2 norm $(\chi_1,\chi_1)_w=\|\chi_1\|_w^2=\int_0^1 w(y)\chi_1^2(y)dy=1$, it follows that

$$\nu_1 = -\nu_{a,1} = -(\|\partial_y\chi_1\|^2 + c\|\chi_1\|^2), \tag{38}$$

where $\|\chi_1\|^2=\int_0^1\chi_1^2(y)dy$ is the usual L^2 norm. From Eqs. (37) and (38), it follows that the norm of the gradient of $\chi_1(y)$ scales as $\|\partial_y\chi_1\|^2\sim O(\alpha_m^{-4})$. This explains the results depicted in Fig. 6. Indeed, this result is significant in the development of simplified perturbation approaches, as discussed in the next paragraph.

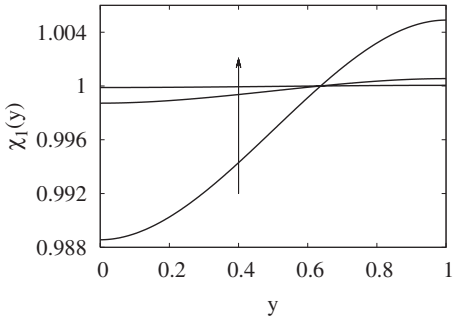

FIG. 6. Dominant eigenfunction $\chi_1(y)$ of the eigenvalue problem Eq. (30) for the shear flow $w(y)=2y$. Arrow indicates increasing values of $\alpha_m=20,60,200$.

C. Regime-based perturbation analysis

The results obtained in the previous paragraph can be summarized as follows: (i) for low Péclet number values, the mixing regime is exclusively controlled by angular diffusion [term $-\varepsilon(4\pi^2/\alpha_m^2)\psi$ in Eq. (23)], (ii) as the Péclet number increases, the effect of angular diffusion becomes progressively negligible and homogenization is controlled by the interplay between transverse diffusion [term $\varepsilon\partial_y^2\psi$ in Eq. (23)] and the cross flow [term $iV(y)\psi$ in Eq. (23)]. Moreover, the dominant eigenfunction $\chi_1(y)$ of Eq. (30) in the absence of cross flow for $\alpha_m>1$ deviates slightly from the uniform profile and this deviation decreases as α_m increases.

Starting from these observations, it is possible to develop a simplified perturbation scheme in which the effects of angular diffusion are decoupled from the other contributions. The starting point is the assumption of the following *decoupling ansatz* for the eigenvalues λ of Eq. (23):

$$\lambda = -\frac{4\pi^2}{\alpha_m^2 \mathrm{Pe}_{\mathrm{eff}}} + \tilde{\lambda}, \tag{39}$$

where $\tilde{\lambda}$ are the eigenvalues of Eq. (23) in the absence of angular diffusion, thus satisfying the eigenvalue problem

$$\tilde{\lambda} w(y)\tilde{\psi}(y) = \varepsilon\partial_y^2\tilde{\psi}(y) + iV(y)\tilde{\psi}(y), \tag{40}$$

where $\tilde{\psi}(y)$ are the associated eigenfunctions. Equation (40) is equipped with the homogeneous Neumann conditions $\partial_y\tilde{\psi}(y)|_{y=0,1}=0$. Indeed, Eqs. (39) and (40) can be viewed as the leading contribution in the perturbative expansion of the eigenvalue and eigenfunctions with respect to $1/\alpha_m^2$.

Equation (40) provides a simplified setting for eigenvalue perturbation and closed-form results can be obtained for generic velocity profiles. To see this, let $\tilde{\nu}=\tilde{\lambda}/\varepsilon=\tilde{\lambda}\,\mathrm{Pe}_{\mathrm{eff}}$, so that Eq. (40) becomes

$$\tilde{\nu} w(y)\tilde{\psi}(y) = \partial_y^2\tilde{\psi}(y) + i\,\mathrm{Pe}_{\mathrm{eff}}V(y)\tilde{\psi}(y) \tag{41}$$

and let us consider $\mathrm{Pe}_{\mathrm{eff}}$ as a small parameter for the perturbation expansion

$$\tilde{\nu} = \sum_{k=0}^{\infty} \mathrm{Pe}_{\mathrm{eff}}^k \tilde{\nu}^{(k)}, \quad \tilde{\psi}(y) = \sum_{k=0}^{\infty} \mathrm{Pe}_{\mathrm{eff}}^k \tilde{\psi}^{(k)}(y). \tag{42}$$

Substituting Eq. (42) into Eq. (41) and collecting term by term equal powers of $\mathrm{Pe}_{\mathrm{eff}}$, one obtains for $k\geq 1$,

$$\partial_y^2\tilde{\psi}^{(k)}(y) + iV(y)\tilde{\psi}^{(k-1)}(y) - w(y)\sum_{h=0}^{k}\tilde{\nu}^{(h)}\tilde{\psi}^{(k-h)}(y) = 0,$$

$$k = 1,2,\ldots, \tag{43}$$

while the equation for the zeroth order term reads as

$$\partial_y^2\tilde{\psi}^{(0)}(y) - w(y)\tilde{\nu}^{(0)}\tilde{\psi}^{(0)}(y) = 0. \tag{44}$$

Each perturbative term $\tilde{\psi}^{(k)}(y)$ should satisfy the boundary conditions $\partial_y\tilde{\psi}^{(k)}(y)|_{y=0,1}=0$, $k=0,1,\ldots$.

Let us focus on the dominant eigenvalue. From Eq. (44), it follows that the dominant eigenvalue is $\nu^{(0)}=0$ and the associated eigenfunction is uniform $\psi^{(0)}(y)=1$. This result is

consistent with the behavior observed for the dominant eigenfunction $\chi_1(y)$ (see Fig. 6) associated with Eq. (30). For the first-order term, Eq. (43) provides $\partial_y^2\tilde{\psi}^{(1)}(y) + iV(y)\psi^{(0)}(y) - w(y)[\tilde{\nu}^{(0)}\psi^{(1)} + \tilde{\nu}^{(1)}\psi^{(0)}] = 0$. By taking into account the result for the zeroth order contribution, this equation simplifies to

$$\partial_y^2\tilde{\psi}^{(1)} = -iV(y) + \tilde{\nu}^{(1)}w(y). \tag{45}$$

A first integration provides

$$\partial_y\tilde{\psi}^{(1)}(y) = -i\int_0^y V(\xi)d\xi + \tilde{\nu}^{(1)}\int_0^y w(\xi)d\xi$$
$$= -iV^{(1)}(y) + \tilde{\nu}^{(1)}w^{(1)}(y), \tag{46}$$

where $V^{(1)}$ and $w^{(1)}(y)$ are the primitives of $V(y)$ and $w(y)$, respectively, such that $V^{(1)}(0) = w^{(1)}(0) = 0$. Observe that the additive constant that should appear after one quadrature has been set equal to zero in order to match the Neumann condition at $y=0$. The enforcement of the boundary condition at $y=1$ provides the value of $\tilde{\nu}^{(1)}$, namely,

$$\tilde{\nu}^{(1)} = i\frac{V^{(1)}(1)}{w^{(1)}(1)} = i\omega_1. \tag{47}$$

The first-order correction to the dominant eigenvalue is therefore purely imaginary. A further quadrature yields $\tilde{\psi}^{(1)}$,

$$\tilde{\psi}^{(1)}(y) = -i\int_0^y V^{(1)}(\xi)d\xi + i\omega_1\int_0^y w^{(1)}(\xi)d\xi$$
$$= i[-V^{(2)}(y) + \omega_1 w^{(2)}(y)] + C_1, \tag{48}$$

where $V^{(2)}(y)$ and $w^{(2)}(y)$ are the primitives of $V^{(1)}(y)$ and $w^{(1)}(y)$. The constant C_1 can be set equal to zero for two reasons: (i) it does not contribute to the shape of the eigenfunction, as any constant value can be rescaled in the uniform zeroth order term, and (ii) it does not contribute to the estimate of $\tilde{\nu}^{(2)}$.

For the second-order expansion, by making use of the above results, one obtains

$$\partial_y^2\tilde{\psi}^{(2)} - [V(y) - \omega_1 w(y)][\omega_1 w^{(2)}(y) - V^{(2)}(y)] - \tilde{\nu}^{(2)}w(y)$$
$$+ iC_1[V(y) - \omega_1 w(y)] = 0. \tag{49}$$

Let

$$G(y) = [V(y) - \omega_1 w(y)][\omega_1 w^{(2)}(y) - V^{(2)}(y)], \tag{50}$$

so that Eq. (49) can be rewritten as

$$\partial_y^2\tilde{\psi}^{(2)}(y) = G(y) + \tilde{\nu}^{(2)}w(y) - iC_1[V(y) - \omega_1 w(y)]. \tag{51}$$

A first quadrature provides

$$\partial_y\tilde{\psi}^{(2)}(y) = G^{(1)}(y) + \tilde{\nu}^{(2)}w^{(1)}(y) - iC_1[V^{(1)}(y) - \omega_1 w^{(1)}(y)], \tag{52}$$

where $G^{(1)}(y) = \int_0^y G(\xi)d\xi$. By enforcing the boundary condition at $y=1$, one obtains the value of $\tilde{\nu}^{(2)}$, namely,

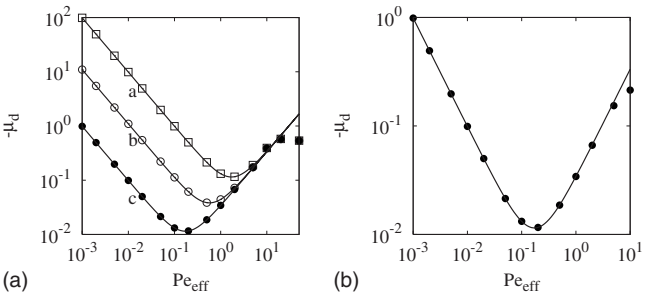

FIG. 7. Perturbative prediction of the real part of the dominant eigenvalue with reversed sign in the low Péclet number range. Panel (a): Poiseuille flow. Symbols (□) refer to $\alpha_m=20$, (○) to $\alpha_m=60$, and (●) to $\alpha_m=200$. Lines (a)–(c) are the theoretical predictions based on Eq. (54). Panel (b): Shear flow. Symbols (●) refer to $\alpha_m=200$. Solid line represents Eq. (54).

$$\tilde{\nu}^{(2)} = -\frac{G^{(1)}(1)}{w^{(1)}(1)}. \tag{53}$$

The second-order correction to the dominant eigenvalue is real. Observe that, because of Eq. (47), the value of C_1 is immaterial since the factor $V^{(1)} - \omega_1 w^{(1)}$ multiplying it is identically equal to zero. A further quadrature of Eq. (52) readily yields the expression for $\tilde{\psi}^{(2)}(y)$.

Since we are mainly interested in the eigenvalue scaling, by collecting Eqs. (39), (42), (47), and (53), the real part μ_d of the dominant eigenvalue up to the second-order reads as

$$\mu_d = \mathrm{Re}[\lambda_d] = -\frac{4\pi^2}{\alpha_m^2\,\mathrm{Pe}_{\mathrm{eff}}} + \frac{\mathrm{Re}[\tilde{\nu}]}{\mathrm{Pe}_{\mathrm{eff}}}$$
$$= -\left(\frac{4\pi^2}{\alpha_m^2\,\mathrm{Pe}_{\mathrm{eff}}} + G^{(1)}(1)\,\mathrm{Pe}_{\mathrm{eff}}\right), \tag{54}$$

where we have made use of the fact that $w^{(1)}(1)=1$, since the axial velocity field is normalized to unit mean velocity.

As can be observed, Eq. (54) resembles a Taylor-Aris-type expression. In the low-intermediate Péclet number region, the scaling of the dominant eigenvalue is given by the superposition of the pure angular contribution, which is inversely proportional to the Péclet number plus a term proportional to $\mathrm{Pe}_{\mathrm{eff}}$ [second term at the right-hand side of Eq. (54)], $-\mu_d = G^{(1)}(1)\,\mathrm{Pe}_{\mathrm{eff}}$. The influence of this second-order correction is depicted in Fig. 2 (line d) and agrees with the observed scaling of the dominant eigenvalue. In the particular case of the Poiseuille flow, the value $G^{(1)}(1)=0.0333$ is obtained.

Figure 7 (panels A and B) shows the overall prediction of the spectral behavior in the low-intermediate Péclet number region for the Poiseuille and the shear flow. A good agreement between the numerical values and the simplified perturbative expansion can be observed. It is worth observing that Eq. (54) is fully predictive once the functional forms of $V(y)$ and $w(y)$ are given and permits to obtain a closed-form expression for the second-order correction in terms of the functional $G^{(1)}(1)$, the value of which depends on the axial and transverse velocity profiles. In principle, one could derive higher-order corrections, which however do not improve sig-

nificantly the results obtained in Fig. 7. This issue and the region of validity of the perturbative expansion are discussed in the next section in the case of a more general perturbative analysis.

IV. FULL PERTURBATIVE SOLUTION AND PHYSICALLY REALIZABLE FLOW SYSTEMS

In the previous paragraph, a decoupling between angular diffusion and the remaining terms in the eigenvalue problem has been enforced in order to derive an approximate perturbative solution that proves in excellent agreement with spectral data. This section provides a full perturbative scheme to approach the spectral properties of Eq. (23) and extends the analysis to physically realizable flow systems.

A. Full perturbative solution

Let us first rewrite Eq. (23) as

$$\mathcal{H}[\psi](y) = \mathcal{H}_0[\psi](y) + i\,\mathrm{Pe}_{\mathrm{eff}} V(y)\psi(y) = \nu w(y)\psi(y), \tag{55}$$

where

$$\mathcal{H}_0 = \frac{d^2}{dy^2} - c, \quad \nu = \lambda\,\mathrm{Pe}_{\mathrm{eff}}, \tag{56}$$

and $c=4\pi^2/\alpha_m^2$. Let $\{\kappa_n\}_{n=1}^{\infty}$ and $\{\phi_n\}_{n=1}^{\infty}$ be the eigenvalue spectrum and the eigenfunction system, respectively, of the operator $\mathcal{H}_0$ weighted with respect to $w(y)$, i.e.,

$$\mathcal{H}_0[\phi_n](y) = \kappa_n w(y)\phi_n(y), \quad n = 1,2,\ldots. \tag{57}$$

The eigenvalues κ_n are real and negative and the eigenfunctions are orthogonal with respect to the weight $w(y)$ [12],

$$(\phi_m,\phi_n)_w = \int_0^1 w(y)\phi_m(y)\phi_n(y)dy = 0, \quad m \neq n. \tag{58}$$

We assume that ϕ_n are normalized, i.e., $(\phi_m,\phi_n)_w=\delta_{m,n}$, and that the eigenvalues are ordered in a decreasing way with respect to n, i.e., $\kappa_1>\kappa_2>\cdots$ (or, equivalently, are ordered decreasingly with respect to their absolute values).

Since $\mathcal{H}|_{\mathrm{Pe}_{\mathrm{eff}}=0}=\mathcal{H}_0$, consider the perturbative continuation of the nth spectral branch by expanding $\psi=\psi_n$ and $\nu=\nu_n$ as

$$\psi_n(y) = \sum_{k=0}^{N_p} \mathrm{Pe}_{\mathrm{eff}}^k \psi_n^{(k)}(y), \quad \nu_n = \sum_{k=0}^{N_p} \mathrm{Pe}_{\mathrm{eff}}^k \nu_n^{(k)}, \tag{59}$$

where

$$\psi_n^{(0)}(y) = \phi_n(y), \quad \nu_n^{(0)} = \kappa_n. \tag{60}$$

Substituting Eq. (59) into Eq. (55), one obtains

$$\mathcal{H}_0[\psi_n^{(k)}](y) + iV(y)\psi_n^{(k-1)}(y) = w(y)\sum_{h=0}^{k} \nu_n^{(h)}\psi_n^{(k-h)}(y), \tag{61}$$

which gives for the first leading terms

$$\mathcal{H}_0[\psi_n^{(0)}](y) = w(y)\nu_n^{(0)}\psi_n^{(0)}(y), \tag{62}$$

$$\mathcal{H}_0[\psi_n^{(1)}](y) + iV(y)\psi_n^{(0)} = w(y)[\nu^{(0)_n}\psi_n^{(1)} + \nu_n^{(1)}\psi_n^{(0)}], \tag{63}$$

$$\mathcal{H}_0[\psi_n^{(2)}](y) + iV(y)\psi_n^{(1)} = w(y)[\nu_n^{(0)}\psi_n^{(2)} + \nu_n^{(1)}\psi_n^{(1)} + \nu_n^{(2)}\psi_n^{(0)}]. \tag{64}$$

By expanding $\psi_n^{(k)}(y)$ with respect to the Laplacian basis $\{\phi_n\}$,

$$\psi_n^{(k)}(y) = \sum_{p\neq n} c_{n,p}^{(k)}\phi_p(y), \tag{65}$$

where we have assumed that $\psi_n^{(k)}$ admit zero projection onto ϕ_n [13], one obtains for the first-order expansion

$$\nu_n^{(1)} = i(V\phi_n,\phi_n), \tag{66}$$

where $(f,g)=\int_0^1 f(y)\bar{g}(y)dy$ is the usual scalar product for complex-valued L^2 functions ($\bar{g}$ is the complex conjugate of g). Equation (66) derives from Eqs. (60) and (63) by taking the inner product of the latter with ϕ_n, since $(\mathcal{H}_0[\psi_n^{(1)}],\phi_n)=0$ and $(\psi_n^{(1)},\phi_n)_w=0$. In a similar way, substituting Eq. (65) into Eq. (63) and taking the scalar product with ϕ_p, $p\neq n$, since

$$(\mathcal{H}_0[\psi_n^{(1)}],\phi_p) = \sum_{q\neq n} c_{n,q}^{(1)}(\mathcal{H}_0[\phi_q],\phi_p) = \sum_{q\neq n} c_{n,q}^{(1)}\kappa_q(\phi_q,\phi_p)_w = c_{n,p}^{(1)}\kappa_p, \tag{67}$$

$(\psi_n^{(0)},\phi_p)_w=(\phi_n,\phi_p)_w=0$, and

$$\nu_n^{(0)}(\psi_n^{(1)},\phi_p)_w = \kappa_n\sum_{q\neq n} c_{n,q}^{(1)}(\phi_q,\phi_p)_w = \kappa_n c_{n,p}^{(1)}, \tag{68}$$

one derives from Eq. (63) the following expression for $c_{n,p}^{(1)}$:

$$c_{n,p}^{(1)} = \frac{i(V\phi_n,\phi_p)}{\kappa_n-\kappa_p}. \tag{69}$$

It can be observed that the first-order eigenvalue correction contributes with a purely imaginary term. In a similar way, for the higher-order corrections, one obtains

$$\nu_n^{(k)} = i(V\psi_n^{(k-1)},\phi_n), \tag{70}$$

which follows from Eq. (61) by taking the product with ϕ_n, observing that $(\mathcal{H}_0[\psi_n^{(k)}],\phi_n)=0$, $k\neq 0$, $\Sigma_{h=0}^{k}\nu_n^{(h)}(\psi_n^{(k-h)},\phi_n)_w=\nu_n^{(k)}(\phi_n,\phi_n)_w=\nu_n^{(k)}$, and

$$c_{n,p}^{(k)} = \frac{1}{\kappa_n-\kappa_q}\left[i\sum_{q\neq n} c_{n,q}^{(k-1)}(V\phi_q,\phi_p) - \sum_{h=1}^{k-1}\nu_n^{(h)}c_{n,q}^{(k-h)}\right], \tag{71}$$

which derives from Eq. (61) by taking the inner product with ϕ_p, $p\neq n$. Specifically, for the second-order eigenvalue correction, Eqs. (69) and (70) determine

$$\nu_n^{(2)} = -\sum_{q\neq n}\frac{(V\phi_n,\phi_q)^2}{\kappa_n-\kappa_q}, \tag{72}$$

which is real.

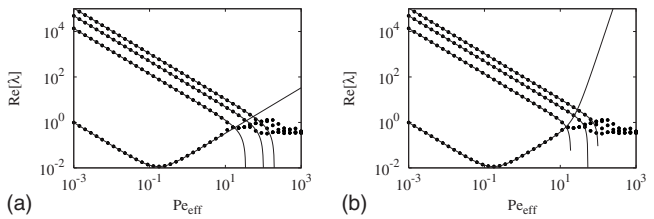

FIG. 8. Perturbative prediction of the real part of the first four eigenvalue branches for the Poiseuille flow at $\alpha_m=200$. Panel (a) $N_p=2$; panel (b) $N_p=6$. Symbols (●) refer to the numerical simulations; continuous lines represent the perturbative prediction.

Let us analyze the results of the complete perturbation scheme. Figure 8 [panel (a)] depicts the results of the perturbation expansion up to the second order ($N_p=2$) for the first four eigenvalue branches in the case of the Poiseuille flow [$w(y)=6y(1-y)$ and $V(y)=-1+2y$]. As can be observed, no significant improvement is obtained by using the full perturbation expansion compared to the simplified approach developed in Sec. III C. Considering the dominant eigenvalue branch, the perturbative solution ceases to be accurate for $\mathrm{Pe}_{\mathrm{eff}}>10^1$, similarly to what is observed in Fig. 7 for the simplified scheme. By increasing the order of the expansion [$N_p=6$, panel (b)], a slight improvement can be observed just close to the crossing of the first two eigenvalue branches (observe that this crossing involves exclusively their real parts) close to $\mathrm{Pe}_{\mathrm{eff}}=10^1$. A further increase of the order N_p does not improve the results. Indeed, the breakup of the perturbative solution should be attributed to the lack of convergence of the power-series expansion Eq. (59) at some critical Péclet number value, related to the lack of analyticity in the behavior of the eigenvalue branches with $\mathrm{Pe}_{\mathrm{eff}}$. This effect can be clearly appreciated by considering the graphs of the imaginary part $\mathrm{Im}[\lambda]$ of the first spectral branches, depicted in Fig. 9 for the Poiseuille flow [this figure shows the imaginary part corresponding to $m=\pm 1$, i.e., to the transverse-flow contribution $\pm iV(y)\psi(y)$ in Eq. (23)]. At the crossing point $\mathrm{Pe}_{\mathrm{eff}}^c\simeq 10^1$ of the real parts of the first two branches, the imaginary parts experience a sudden increase, which corresponds to an unbounded value of $d\ \mathrm{Im}[\lambda]/d\ \mathrm{Pe}_{\mathrm{eff}}$ evaluated at $\mathrm{Pe}_{\mathrm{eff}}=\mathrm{Pe}_{\mathrm{eff}}^c$. This phenomenon is an intrinsic property of the spectrum, which limits the applicability of the power-series expansion up to value of the effective Péclet number smaller than $\mathrm{Pe}_{\mathrm{eff}}^c$.

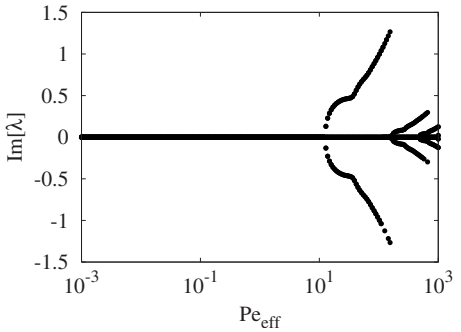

FIG. 9. Imaginary part of the first eigenvalue branches for the Poiseuille flow at $\alpha_m=200$.

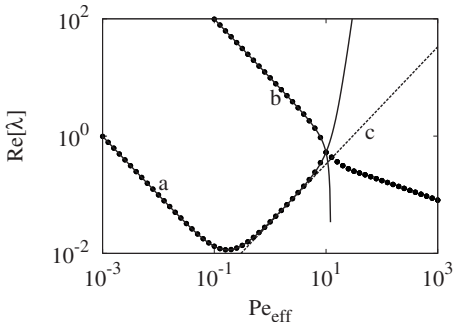

FIG. 10. Perturbative prediction of the real part of the first two eigenvalue branches [lines (a) and (b) for $N_p=6$] for the simple shear flow $w(y)=1$, $V(y)=2y$ at $\alpha_m=200$. Symbols (●) correspond to the numerical simulations. Dotted line (c) is the second-order prediction of the simplified perturbation scheme Eq. (54).

So far, we have analyzed the case where $w(y)$ is nonuniform [possessing a quadratic (Poiseuille) or a linear (Couette) shape]. As discussed in Sec. III, this corresponds physically to the stationary homogenization dynamics in an inflow-outflow three-dimensional mixer unit along the axial coordinate. The analysis developed applies straightforwardly also in the case $w(y)=1$, which physically corresponds to the dynamic response of a two-dimensional Couette system possessing a small gap between inner and outer cylinders and the results obtained are qualitatively similar to those depicted in Figs. 7 and 8. As an example, Fig. 10 shows the simplified perturbative prediction of the behavior of the dominant branch obtained by applying the method developed in Sec. III C, while lines (a) and (b) represent the results of the full perturbation scheme with $N_p=6$. Higher-order expansions provide slightly better results than the simplified model Eq. (54) solely in a small neighborhood of the crossing point $\mathrm{Pe}_{\mathrm{eff}}^c$.

B. Perturbation analysis of physically realizable mixing systems: The lid-driven cavity

The same perturbative approach developed in the previous section for advection-diffusion problems expressed by a non-Hermitian Schrödinger operator in the presence of an imaginary potential can be extended to generic autonomous flows. In this case, the spectral problem associated with the advection-diffusion equation takes the form

$$-\mathbf{v}(\mathbf{x})\cdot\nabla\psi(\mathbf{x})+\mathrm{Pe}^{-1}\nabla^2\psi(\mathbf{x})=\lambda\psi(\mathbf{x}),\quad \mathbf{x}\in\Omega, \tag{73}$$

where Ω is a bounded domain, the flow is incompresssible, $\nabla\cdot\mathbf{v}=0$, and the normal component of the velocity field vanishes at the boundary $\partial\Omega$ of the mixing domain. Equation (73) is equipped with the homogeneous Neumann condition at the boundary $\partial\psi/\partial n|_{\partial\Omega}=0$.

Letting $\nu=\lambda\ \mathrm{Pe}$, Eq. (73) can be rewritten as

$$-\mathrm{Pe}\ \mathbf{v}(\mathbf{x})\ \nabla\ \psi(\mathbf{x})+\nabla^2\psi(\mathbf{x})=\nu\psi(\mathbf{x}). \tag{74}$$

By applying the expansion Eq. (59) with Pe in place of $\mathrm{Pe}_{\mathrm{eff}}$, one obtains for the zeroth-order term

$$\nabla^2 \psi_n^{(0)} = \nu_n^{(0)} \psi_n^{(0)}, \tag{75}$$

indicating that $\nu_n^{(0)}$ equals the nth eigenvalue κ_n of the Laplacian operator in Ω and $\psi_n^{(0)} = \phi_n$ is the associated eigenfunction. Henceforth, we assume that $(\phi_n, \phi_m) = \delta_{n,m}$ for $n \neq m$. For the first- and second-order terms, the perturbative equations read

$$-\mathbf{v} \cdot \nabla \psi_n^{(0)} + \nabla^2 \psi_n^{(1)} = \nu_n^{(0)} \psi_n^{(1)} + \nu_n^{(1)} \psi_n^{(0)}, \tag{76}$$

$$-\mathbf{v} \cdot \nabla \psi_n^{(1)} + \nabla^2 \psi_n^{(2)} = \nu_n^{(0)} \psi_n^{(2)} + \nu_n^{(1)} \psi_n^{(1)} + \nu_n^{(2)} \psi_n^{(0)}. \tag{77}$$

By expressing $\psi_n^{(0)}$ with respect to the Laplacian basis $\{\phi_n\}$ via Eq. (65), one obtains for $\nu_n^{(1)}$ the expression

$$\nu_n^{(1)} = -(\phi_n, \mathbf{v} \cdot \nabla \phi_n) = 0, \tag{78}$$

which is identically equal to zero since

$$(\phi_n, \mathbf{v} \cdot \nabla \phi_n) = \int_\Omega \phi_n \mathbf{v} \cdot \nabla \phi_n d\mathbf{x} = \frac{1}{2} \int_\Omega \mathbf{v} \cdot \nabla \phi_n^2 d\mathbf{x}$$
$$= \frac{1}{2} \int_\Omega \nabla (\mathbf{v} \phi_n^2) d\mathbf{x} = \frac{1}{2} \int_{\partial\Omega} \phi_n^2 \mathbf{v} \cdot \mathbf{n} dS = 0, \tag{79}$$

where $\mathbf{n}$ is the normal unit vector, outwardly oriented, at $\partial\Omega$. By applying the same approach described in the previous section, the expression for the first-order coefficient $c_{n,p}^{(1)}$ entering Eq. (65) reads as

$$c_{n,p}^{(1)} = -\frac{(\mathbf{v} \cdot \nabla \phi_n, \phi_p)}{\kappa_n - \kappa_p}. \tag{80}$$

For the second-order term in the eigenvalue expansion, the inner product of Eq. (77) with ϕ_n provides for $\nu_n^{(2)}$ the following expression:

$$\nu_n^{(2)} = -(\phi_n, \mathbf{v} \cdot \nabla \psi_n^{(1)})$$
$$= -\sum_{m \neq n} c_{n,m}^{(1)} (\phi_n, \mathbf{v} \cdot \nabla \phi_m)$$
$$= -\sum_{m \neq n} \frac{(\phi_n, \mathbf{v} \cdot \nabla \phi_m)^2}{\kappa_n - \kappa_m}. \tag{81}$$

As a case study, consider the flow in a two-dimensional (2D) lid-driven cavity in the creeping flow regime. Let L_x and L_y be the lengths of the two edges of the cavity with $L_x/L_y = \alpha > 1$ and let the upper (parallel to the x axis) wall move with uniform tangential velocity V_w. In this case, the Péclet number is defined with respect to the wall velocity as $\mathrm{Pe} = V_w L_x / D$, so that the nondimensional velocity $\mathbf{v}$ entering Eq. (73) possesses unit tangential velocity at the moving wall. The velocity field $\mathbf{v}$ has been obtained by using a finite-element code enforcing the stream-function/vorticity formulation.

Let $\mathbf{x} = (x, y)$ be the nondimensional Cartesian coordinate system obtained by rescaling x and y by the length of the corresponding edges $x \mapsto x/L_x$ and $y \mapsto y/Ly$, so that $\Omega = (0,1) \times (0,1)$ in the nondimensional formulation. The Laplacian operator in the nondimensional coordinate system (x, y) reads as

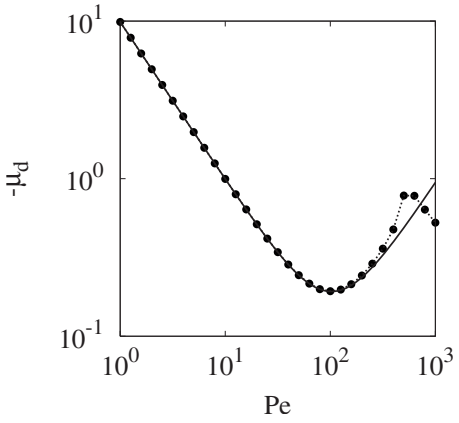

FIG. 11. Perturbative prediction of the real part of the dominant eigenvalue for the 2D cavity flow with $\alpha = 10$. Symbols (●) refer to the numerical simulations; continuous line represents the perturbative prediction

$$\nabla^2 = \partial_x^2 + \alpha^2 \partial_y^2. \tag{82}$$

The dominant eigenfunction of the pure diffusive case ($\mathrm{Pe} = 0$) is given by $\phi_1(x) = \cos(\pi x)$, so that its continuation as a function of the Péclet number represents the dominant spectral branch in the low and intermediate Péclet number regions (beside the zero eigenvalue associated with mass conservation). Figure 11 depicts the comparison between the real part μ_d of the dominant eigenvalue obtained, from direct solution of the eigenvalue problem Eq. (73) and the results of the perturbative expansion Eqs. (59), (78), and (81). The results shown in Fig. 11 are qualitatively similar to those obtained for the rectified Couette flow (see Fig. 7) and indicate that the perturbative analysis developed in this section can be successfully applied for generic autonomous flows in the low and intermediate Péclet number regions.

V. CONCLUDING REMARKS

Perturbation techniques provide a valuable tool for addressing dispersion and mixing properties of passive scalar in laminar flows. The use of physical reasoning, aimed at identifying which contribution controls the homogenization process in which Péclet number region, permits to simplify the analysis. Specifically, we have addressed in detail a simplified perturbation method that, based on the negligible role of angular diffusion in the intermediate Péclet number region, permits to predict quantitatively, without the use of any adjustable parameter, the behavior of the dominant eigenvalue as a function of the Péclet number. In point of fact, the method described in Sec. III C yields an analytical expression for the *Taylor correction* [factor $G^{(1)}(1)\,\mathrm{Pe}_{\mathrm{eff}}$ in Eq. (54)] as a functional of the axial and angular velocities. The development of a more rigorous, but more elaborate, perturbation scheme (see Sec. IV) does not improve significantly either qualitatively or quantitatively the results obtained by means of the simplified scheme.

Throughout this paper, we have considered, as a model system, a Cartesian version of an open Couette flow, in

which the action of angular diffusion is expressed by means of the imaginary potential term $iV(y)\psi(y)$ in Eq. (23). In this formulation, the perturbed operator is $\mathcal{H}=\mathcal{H}_0+i\,\mathrm{Pe}_{\mathrm{eff}}V(y)$, where $\mathcal{H}_0=\partial_y^2$. The same approach, both in the form of the simplified perturbation scheme described in Sec. III C and in the complete expansion (Sec. IV), can be applied to more complex autonomous flows in arbitrary geometries, for which the perturbed operator takes the form $\mathcal{H}=\mathcal{H}_0+\mathrm{Pe}_{\mathrm{eff}}\mathcal{V}$, where $\mathcal{H}_0=\nabla^2$ and $\mathcal{V}=-\mathbf{v}\cdot\nabla$, where $\mathbf{v}$ is an autonomous flow field. This has been addressed in Sec. IV by considering the 2D lid-driven cavity flow as a model system.

We have also addressed the limitations of the perturbation methods in the study of the properties of non-Hermitian operators associated with advection-diffusion processes. These limitations are, in some sense, intrinsic to the spectral structure of these operators, as discussed in the case study in Sec. IV, and are associated with the breakup of analyticity of the eigenvalue expansion at some characteristic point $\mathrm{Pe}_{\mathrm{eff}}^c$, corresponding to the collision of the real parts of two eigenvalue branches.

The fact that perturbation analysis provides an accurate description of the spectral properties in the low and intermediate Péclet number regions admits practical implications in the quantification of mixing. In point of fact, the dominant eigenvalue of the convection-enhanced branch is inversely proportional to the characteristic mixing time in all the cases where the initial (for closed systems) or inlet (for open systems) conditions do not excite eigenmodes of the diffusive branch [14]. Therefore, the analytical estimate of the dominant eigenvalue by perturbation analysis constitutes a simple way for predicting the characteristic mixing times in these cases.

[1] N.-T. Nguyen and S. T. Wereley, *Fundamentals And Applications of Microfluidics*, 2nd ed. (Artech House, Boston, 2006); J. Berthier, P. Silberzan, *Microfluidics for Biotechnology* (Artech House, Boston, 2005); N.-T. Nguyen and Z. Wu. J. Micromech. Microeng. **15**, R1 (2005).

[2] A. J. Majda and P. R. Kramer, Phys. Rep. **314**, 237 (1999); I. Scheuring, G. Karolyi, A. Pentek, T. Tel, and Z. Toroczkai, Freshwater Biol. **45**, 123 (2000); B. I. Shraiman and E. D. Siggia, Nature (London) **405**, 639 (2000); D. Perugini, G. Poli, and R. Mazzuoli, J. Volcanol. Geotherm. Res. **124**, 255 (2003).

[3] A. Gelb, J. P. Gleeson, J. West, and O. M. Roche, SIAM J. Appl. Math. **64**, 1294 (2004); A. Ajdari, N. Bontoux, and H. Stone, Anal. Chem. **78**, 387 (2006).

[4] R. F. Ismagilov, A. D. Stroock, P. J. A. Kenis, G. Whitesides, and H. A. Stone, Appl. Phys. Lett. **76**, 2376 (2000); J.-B. Salmon and A. Ajdari, J. Appl. Phys. **101**, 074902 (2007).

[5] A. Adrover, S. Cerbelli, F. Garofalo, and M. Giona, 2nd Micro-nano Flows Conference, West London, September 2009 (unpublished).

[6] G. Taylor, Proc R. Soc. London, Ser. A **219**, 186 (1953); R. Aris, Proc. R. Soc. London, Ser. A **235**, 67 (1956); Y. Ananthakrishnan, W. N. Gill, and A. J. Barduhn, AIChE J. **11**, 1063 (1965).

[7] M. Giona, S. Cerbelli, and F. Garofalo, Europhys. Lett. **83**, 34001 (2008).

[8] R. Smith, J. Fluid Mech. **130**, 299 (1983); M. D. Bryden and H. Brenner, *ibid.* **311**, 343 (1996).

[9] G. Karniadakis, A. Beskok, and N. Aluru, *Microflows and Nanoflows: Fundamentals and Simulation* (Springer Verlag, New York, 2005); T. M. Squires and S. R. Quake, Rev. Mod. Phys. **77**, 977 (2005); R. B. Schoch, J. Han, and P. Renaud, *ibid.* **80**, 839 (2008).

[10] H. Zhao and H. H. Bau, Anal. Chem. **79**, 7792 (2007).

[11] The eigenvalues and eigenfunctions have been obtained numerically by expanding $\psi(y)$ in cosine basis, $\psi(y)=\Sigma_{k=0}^{N}x_k\cos(k\pi y)$, and by solving the generalized eigenvalue problem associated with Eq. (23).

[12] M. Giona, A. Adrover, and S. Cerbelli, Phys. Rev. E **80**, 066302 (2009).

[13] L. D. Landau and E. M. Lifschitz, *Quantum Mechanics (Non-Relativistic Theory)*, 3rd ed. (Pergamon, Oxford, 1977).

[14] M. Giona, in *Analysis and Control of Mixing with an Application to Micro and Macro Flow Processes*, edited by L. Cortelezzi and I. Mezić (Springer, Wien, 2009); M. Giona, A. Paglianti, S. Cerbelli, S. Pintus, and A. Adrover, Can. J. Chem. Eng. **80**, 580 (2002).